Investigating Computational Geometry for Failure Prognostics in Presence of Imprecise Health Indicator: Results and Comparisons on C-MAPSS Datasets

Emmanuel Ramasso

FEMTO-ST Institute
Department of Automatic Control and Micro-Mechatronic Systems,
Department of Applied Mechanics,
UMR CNRS 6174 - UFC / ENSMM / UTBM, 25000, Besançon, France
emmanuel.ramasso@femto-st.fr

ABSTRACT

Prognostics and Health Management (PHM) is a multidisciplinary field aiming at maintaining physical systems in their optimal functioning conditions. The system under study is assumed to be monitored by sensors from which are obtained measurements reflecting the system's health state. A health index (HI) is estimated to feed a data-driven PHM solution developed to predict the remaining useful life (RUL). In this paper, the values taken by an HI are assumed imprecise (IHI). An IHI is interpreted as a planar figure called polygon and a case-based reasoning (CBR) approach is adapted to estimate the RUL. This adaptation makes use of computational geometry tools in order to estimate the nearest cases to a given testing instance. The proposed algorithm called RULCLIPPER is assessed and compared on datasets generated by the NASA's turbofan simulator (C-MAPSS) including the four turbofan testing datasets and the two testing datasets of the PHM'08 data challenge. These datasets represent 1360 testing instances and cover different realistic and difficult cases considering operating conditions and fault modes with unknown characteristics. The problem of feature selection, health index estimation, RUL fusion and ensembles are also tackled. The proposed algorithm is shown to be efficient with few parameter tuning on all datasets.

1. INTRODUCTION

Knowledge-based systems and Case-Based Reasoning approaches (CBR) have appeared as suitable tools for data-driven Prognostics and Health Management (PHM) (Saxena, Wu, & Vachtsevanos, 2005; T. Wang, Yu, Siegel, & Lee, 2008; T. Wang, 2010; Ramasso, Rombaut, & Zerhouni, 2013). In CBR, historical instances of the system - with condition data and known failure time - are used to create a library of degradation models or health indices. Then, for a test instance, the similarity with the degradation models is evaluated generating a set of *Remaining Useful Life* (RUL) estimates which are finally aggregated.

The required assumptions for CBR implementation are limited, the main issues consisting in, on the one hand, the choice of an appropriate similarity measure and, on the other hand, the selection of the relevant training instances. CBR approaches are also flexible since it is simple to incorporate quantitative and qualitative pieces of knowledge such as measurements and expertise.

We consider applications for which the noise due to various sources, such as operational conditions or fault modes, can not be well characterised and where filtering may change the meaning of the health index. We assume that the health index can not be well defined by a single real value but only by *Imprecise Health Index* (IHI). To fix ideas, an illustration taken from the turbofan engine dataset (Saxena, Goebel, Simon, & Eklund, 2008) (used and detailed in experiments) is given in Figure 1. The figure pictorially represents the IHI taken from the fourth dataset (made of two fault modes and six operating conditions) for the 8th training data (P_1), the 100th training data (P_2) and the 1st testing data (P_3) of this dataset. As depicted, fault modes may generate

- sudden changes in wear (e.g in P_1, $t \in [225, 275]$) that may increase the lifetime of the unit. It may be due to both fault modes and operating conditions, for example a drastic decrease of speed to cope with mechanical incidents or meteorological phenomenons.
- Unexpected changes in the trend, such as increasing instead of decreasing (e.g. P_2, $t > 125$) that may disturb the algorithm. It may be due to component failures such

as sensors or electronics.

- Sudden bursts characterised by low signal-to-noise ratio (SNR) on a possibly short duration which deeply affect the HI (e.g. on P_3 with $t \in [10, 75]$) that may affect the lifetime accordingly to the fault type which is generally unknown.

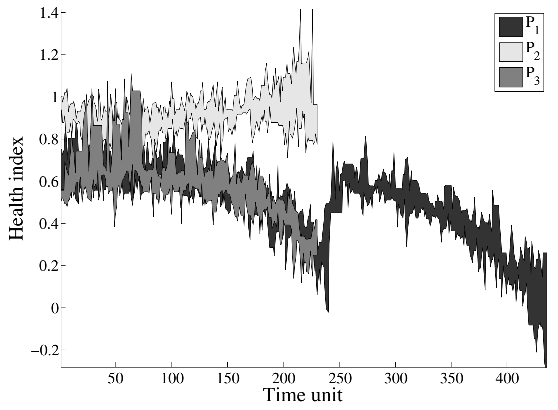

Figure 1. Effect of fault modes and operating conditions on health indices estimation. HIs (here obtained from training instances) are described with planar figures called polygons.

The representation and the propagation of imprecision (or uncertainty) is of paramount importance in engineering analyses (Vachtsevanos, 2006; Orchard, Kacprzynski, Goebel, Saha, & Vachtsevanos, 2008; Beer, Ferson, & Kreinovich, 2013). Several mathematical theories (Klir & Wierman, 1999) have been used in prognostics such as probability theory (including Bayesian approaches) (Peng et al., 2012), set-membership approaches (including fuzzy-sets) (Chen, Zhang, Vachtsevanos, & Orchard, 2011; El-Koujok, Gouriveau, & Zerhouni, 2011) and Dempster-Shafer's theory of belief functions (Serir, Ramasso, & Zerhouni, 2012; Ramasso et al., 2013). Facing imprecision in HIs for prognostics is thus not new but the way to handle it can be considered differently.

We assume 1-D health index to be available but obtained from noisy measurements. The data points are supposed to represent vertices of a simple planar polygon. The IHI is thus a polygon-shaped health index represented by a planar figure. Three polygons are depicted in Figure 1. Using computational geometry tools, a prognostics method is proposed that handles IHI without knowing nor estimating the noise properties. The method is based on CBR for which a similarity measure adapted to IHI and polygon is developed. The set of cases is made of training instances represented by polygons and the similarity with a testing instance recorded on the in-service system is made dependent on the degree of *intersection* between both training and testing polygon instances. The prognostics algorithm introduced is called "RULCLIPPER" (Remaining Useful Life estimation based on impreCise heaLth Index modeled by Planar Polygons and similarity-basEd Reasoning").

The next Section is dedicated to the presentation of a methodology to build imprecise health index and perform prognostics. The methodology is then applied on C-MAPSS datasets.

2. PROGNOSTICS BASED ON IMPRECISE HEALTH INDEX: A CBR APPROACH

A health index (HI) takes the form of a 1-dimensional real-valued signal $H = [x_1\ x_2 \ldots\ x_j \ldots\ x_T]^{\mathsf{T}}, x_j \in \mathbb{R}$ obtained at some instants $t_1,\ t_2 \ldots\ t_T$.

2.1. Polygon-shaped representation of IHI

An IHI is defined as a polygon where each vertex is represented by a data point estimated from the original HI. The set of vertices is obtained by first rearranging the data points to define an ordered sequence that is made possible by extracting the upper and lower envelopes of the noisy HI. For that, let's define $\tilde{H} = [\tilde{x}_1\ \tilde{x}_2 \ldots\ \tilde{x}_j \ldots\ \tilde{x}_T]^{\mathsf{T}}$ a smooth HI obtained by applying a *filter* over H such that the extraction of both envelopes of H is made *easier*. The filter used in this paper was a 15-point moving average.

A polygon (representing an IHI) is thus defined as a set of pairs (x_j, t_j) made of HI values x_j at time index t_j.

The upper envelope of H denoted $\mathcal{S}$ is defined by

$$\mathcal{S} = \{(x_j, t_j) | x_j \geq \tilde{x}_j\} \cup \{(x_{j-1}, t_j) | x_j < \tilde{x}_j\}\ , \tag{1}$$

meaning that, for a given data point j, if the HI value x_j at time t_j is greater than the filtered value $\tilde{x}_j$ then the upper envelope is equal to the HI value, otherwise it takes its previous value. The lower envelope $\mathcal{I}$ is defined similarly by

$$\mathcal{I} = \{(x_j, t_j) | x_j < \tilde{x}_j\} \cup \{(x_{j-1}, t_j) | x_j \geq \tilde{x}_j\}\ . \tag{2}$$

The ordered pairs of vertices listed counterclockwise represents a bounding closed polygonal chain that separates the plane into two regions. The word "polygon" refers to a plane figure bounded by the closed path defined as:

$$\begin{aligned}\mathcal{P} = \big\{&(x_1, t_1)^{\mathcal{S}}, (x_2, t_2)^{\mathcal{S}} \ldots\ (x_j, t_j)^{\mathcal{S}} \ldots\ (x_T, t_T)^{\mathcal{S}},\\ &(x_T, t_T)^{\mathcal{I}}, (x_{T-1}, t_{T-1})^{\mathcal{I}} \ldots\ (x_1, t_1)^{\mathcal{I}}, (x_1, t_1)^{\mathcal{S}}\big\}\end{aligned} \tag{3}$$

with $(x_j, t_j)^{\mathcal{S}} \in \mathcal{S}$ and $(x_j, t_j)^{\mathcal{I}} \in \mathcal{I}$. To close the polygon, the first and last vertices are the same. The pairs of vertices define a finite sequence of straight line segments representing the polygon.

More specifically, a polygon is a region of the plane enclosed by a simple cycle of straight line segments where nonadjacent segments do not intersect and two adjacent segments intersect only at their common endpoint (Rosen, 2004). However, the second part of the definition of the bounds may generate some segment intersections. These inconsistencies can be corrected easily by exchanging the corresponding values of the lower and upper bounds when an intersection is detected. When consistent bounds are obtained, the polygon is made of non-intersecting line segments which characterise a Jordan's simple closed curve also called *simple* polygon (Filippov, 1950). This category of polygon enables one to apply some standard algorithms from Computational Geometry (Rigaux, Scholl, & Voisard, 2002; Rosen, 2004; Longley, de Smith, & Goodchild, 2007). Note that some of the most efficient algorithms for operations on polygons can manage self-intersections (Vatti, 1992; Greiner & Hormann, 1998) but these inconsistencies generally increase time-consumption.

2.2. CBR approach for prognostics based on IHI

2.2.1. Training dataset

We assume the training dataset to be composed of N training instances:

$$\mathcal{L} = \{\mathcal{P}_i, \mathcal{K}_i\}_{i=1}^{N} \tag{4}$$

where $\mathcal{P}_i$ is the ith polygon attached to the ith imprecise health index H_i and $\mathcal{K}_i = [y_1 \;\; y_2 \ldots \;\; y_j \ldots \;\; y_T]^{\mathrm{T}}, y_j \in \mathbb{N}$ represents a discrete-valued signal reflecting a system's state. The component $\mathcal{K}_i$ may be useful in some applications where the system can be described by means of latent variables (Ramasso & Denoeux, 2013; Javed, Gouriveau, & Zerhouni, 2013). In that case, $\mathcal{K}_i$ may represent a partial knowledge about the state. For example, in (Ramasso et al., 2013), partial knowledge was encoded by belief functions to express imprecision and uncertainty about the states.

2.2.2. Determining the nearest case

A testing instance takes the form of a health index H^* from which the envelopes can be estimated as explained in the previous paragraph, leading to the polygon representation $\mathcal{P}_*$. As in usual CBR approaches for prognostics (T. Wang, 2010; Ramasso et al., 2013), the goal is to sort the training instances with respect to their similarity to the testing instance. However, since the training instances are made of polygons, the usual Euclidean distance is not adapted. We propose the following similarity measure.

Getting inspired from the Computer Vision community (Powers, 2011), recall, precision and F_β indices are used to quantify the relevance of a training instance compared to the testing one. Precision represents the fraction of the retrieved instance that is relevant, while recall is the fraction of the relevant instance that is retrieved. The F_β is an harmonic mean which gives equal weight to recall and precision when $\beta = 1$. Note that the three indices are normalised into $[0, 1]$.

More precisely, for the ith training instance:

1. Estimate the area of the intersection between the polygon $\mathcal{P}_i$ and $\mathcal{P}_*$:
$$\mathcal{A}_\cap = \text{Area}\,(\mathcal{P}_i \cap \mathcal{P}_*) \tag{5}$$
2. Compute the "recall":
$$R_{\text{ec}} = \frac{\mathcal{A}_\cap}{\mathcal{A}_i} \tag{6}$$
3. Compute the "precision":
$$P_{\text{rec}} = \frac{\mathcal{A}_\cap}{\mathcal{A}_*} \tag{7}$$
4. Compute the "$\mathrm{F}_{\beta,i}$", in particular for $\beta = 1$, characterizing the similarity with the ith training instance:
$$F_{1,i} = 2\frac{R_{\text{ec}} \cdot P_{\text{rec}}}{R_{\text{ec}} + P_{\text{rec}}} \tag{8}$$

where $\mathcal{A}_i, \mathcal{A}_*, \mathcal{A}_\cap$ represent the area of polygons $\mathcal{P}_i$, $\mathcal{P}_*$ and of their intersection respectively.

Example 1 *An illustration of intersection is given in Figure 2 where the darkest polygon represents a training instance and the two other polygons are testing ones. The whitest polygon is within the testing instance meaning that the precision is high, but the recall is pretty low since it covers only a small part of the testing instance. On the opposite, the third polygon covers entirely the testing instance leading to a high recall but its spread decreases the precision.*

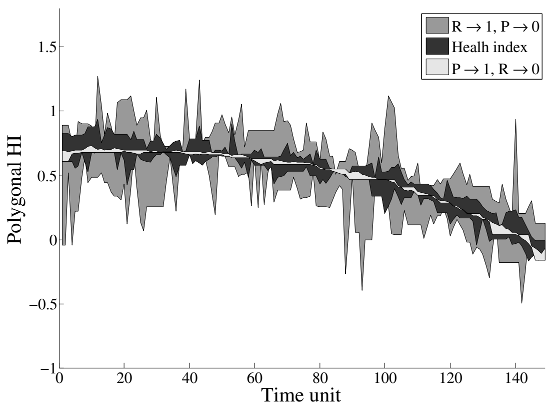

Figure 2. Illustration of recall and precision.

Practically, intersection construction is the main difficulty and was tackled quite recently in computational geometry for arbitrary planar polygons. It consists in determining the region of geometric intersection which can be performed in three phases (Rosen, 2004) (Chap. 38):

1. Compute the intersection between the boundaries of the objects using the linearithmic plane sweep algorithm (Bentley & Ottmann, 1979);
2. If the boundaries do not intersect then determine whether one object is nested within the other;
3. If the boundaries do intersect then classify the resulting boundary fragments gathered to create the final intersec-

tion region (Margalit & Knott, 1989; Chazelle & Edelsbrunner, 1992), which can be performed in linearithmic time. Regularized Boolean operations ensure the closure of the interior of the set-theoretic intersection.

In this paper, the Vatti's algorithm (Vatti, 1992) has been used because it is generic and can manage most of pratical cases. Several implementations of this algorithm have been proposed, especially in (Greiner & Hormann, 1998) which was shown to be particularly efficient.

2.2.3. Estimating the Remaining Useful Life (RUL)

The F_1 measure is used to sort the N training polygon instances in descending order: $\mathcal{P}_{(1)} > \mathcal{P}_{(2)} \cdots > \mathcal{P}_{(j)} \cdots > \mathcal{P}_{(N)}$ so that $\mathcal{P}_{(1)}$ is the closest instance to the testing one and $\mathcal{P}_{(N)}$ the farthest one. The index (i) in $\mathcal{P}_{(i)}$ represents a reordering and the symbol $>$ in $\mathcal{P}_{(i)} > \mathcal{P}_{(j)}$ means that the ith polygon is more similar to the testing instance that the jth.

CBR assumes that a limited number of instances, say K, are enough to approximate the testing instance. The K closest training instances can then be combined to estimate the RUL. The length of a training instance minus the length of a testing instance provides an estimation of the RUL (Figure 3). Given the definition of a polygon (Section 2.1) and of the training dataset (Eq. 4), the length of both the training and testing polygon instances is given by T_i and T_* respectively. Therefore, the estimated RUL is given by

$$\hat{\text{RUL}} = T_i - T_* \ . \tag{9}$$

Example 2 *Two polygons are illustrated in Figure 3, one coming from the training dataset $\#1$ (the tenth instance) and one from the testing dataset $\#1$ (the first instance). Since $T_1 = 222$ and $T_* = 31$, the estimated RUL is 191 time-units.*

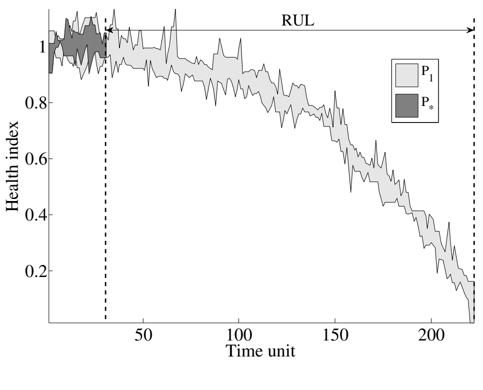

Figure 3. Polygon instances: training ($\mathcal{P}_1$) and testing ($\mathcal{P}_*$).

Each closest training instance $\mathcal{P}_{(i)}$ can be accompanied by a state sequence $\mathcal{K}_{(i)}$ so that K estimations of the RUL, denoted $\hat{\text{RUL}}_{\mathcal{K}}$, can be obtained from the state sequences in addition to the ones obtained with $\mathcal{P}_{(i)}$ and denoted $\hat{\text{RUL}}_{\mathcal{P}}$. Using $\mathcal{K}_{(i)}$, the last transition in the sequence is supposed to represent a jump of the system to a faulty state. This assumption relies on the fact that the last part of a training instance represents the system's end-of-life (Ramasso et al., 2013; Ramasso & Gouriveau, 2013; Javed et al., 2013).

The $2K$ estimations of the RUL can then be pooled in one set: $\hat{\text{RUL}}_{\mathcal{PK}} = \{\hat{\text{RUL}}_{\mathcal{P}}, \hat{\text{RUL}}_{\mathcal{K}}\}$ and an information fusion process can then be performed to combine these partial RUL estimates. According to the application, the fusion rule can be adapted (Kuncheva, 2004).

A plot chart of RULCLIPPER algorithm is depicted in Figure 4. Some of the elements will be illustrated in the next section dedicated to experiments.

3. EXPERIMENTS: METHOD

RULCLIPPER is tested on the datasets obtained from the turbofan engine degradation simulator (Saxena, Goebel, et al., 2008). Before presenting results, several details about the datasets have to be presented, in particular how to select the features and how to compute the health index.

3.1. Turbofan engine degradation simulator

The simulation model (Saxena, Goebel, et al., 2008) was built on the Commercial Modular Aero-Propulsion System Simulation (C-MAPSS) developed at NASA Army Research Lab., able to simulate the operation of an engine model of the 90.000 lb thrust class. A total of 21 output variables were recorded to simulate sensor measurements to the system. Another 3 variables representing the engine operating conditions were recorded, namely altitude (kilo feet), Mach number (speed) and Throttle Resolver Angle (TRA) value which is the angular deflection of the pilot's power lever having a range from 20% to 100%. In the sequel, references to variables are made by using their column position in the data files as provided on the data repository of the Prognostics Center of Excellence website: it begins by number 6 and finishes to 26 (see (Saxena, Goebel, et al., 2008) for details).

3.2. Datasets

Six datasets generated from independent simulation experiments were provided, each with some specificities (Saxena, Goebel, et al., 2008).

Datasets $\#1$ and $\#2$ include only one fault modes (HPC degradation) while datasets $\#3$ and $\#4$ include two (HPC degradation and fan degradation). Datasets $\#1$ and $\#3$ include a single operational condition against six for datasets $\#2$ and $\#4$. Dataset $\#4$ represents the most complex case study. Datasets $\#5_T$ (semi-final **t**esting dataset) and $\#5_V$ (final **v**alidation dataset) were generated for the 2008's PHM data challenge with one fault mode and six operating conditions. The two last datasets have common training instances. A summary of

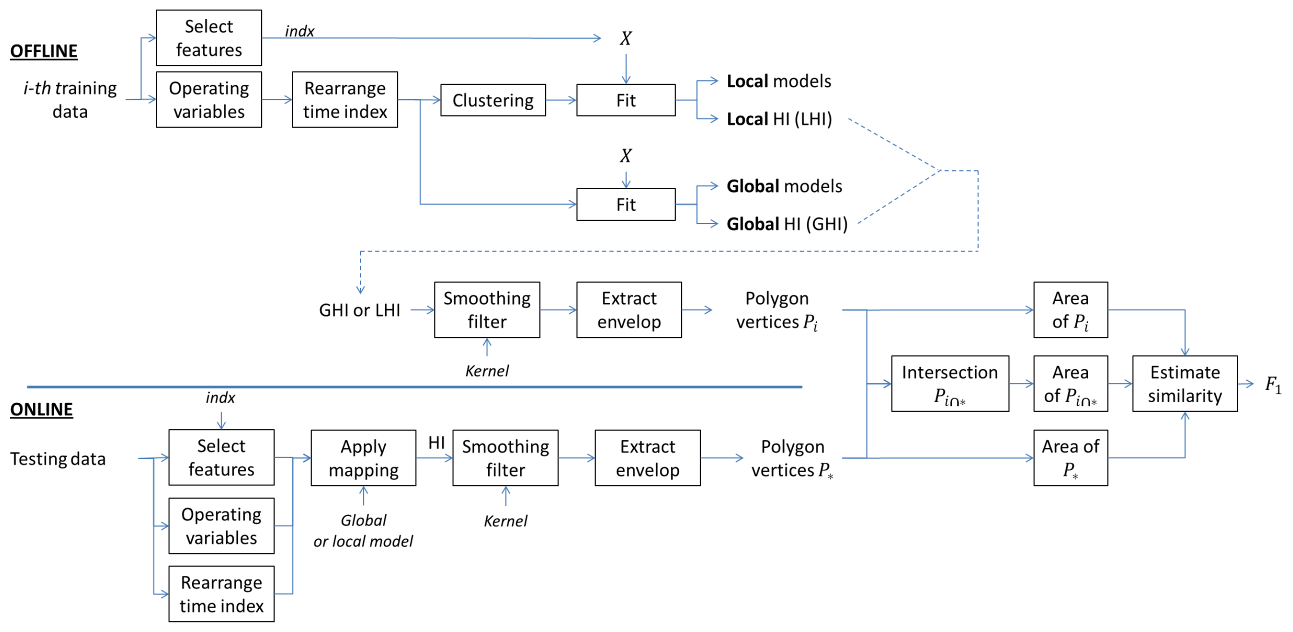

Figure 4. The sequence of operations involved in the proposed approach.

the six datasets are shown in Table 1 according to information taken from (Saxena, Goebel, et al., 2008).

Each dataset is divided into training and testing subsets. The training set includes instances with complete run-to-failure data (to develop life prediction models), and the actual failure mode for training instances in $\#3$ and $\#4$ is not labeled. The testing datasets include instances with data up to a certain cycle and are used for RUL estimation and algorithm performance evaluation.

The testing instances are also simulated run-to-failure and only an earlier portion of the history is provided. The actual life (RUL) of the testing instances are known only for datasets $\#1$, $\#2$, $\#3$ and $\#4$ and can only be used for testing algorithm. For datasets $\#5_T$ and $\#5_V$, results have to be uploaded to the data repository: uploading is allowed only once a day for $\#5_T$ whereas only a single try is possible for dataset $\#5_V$.

The validation can be performed by many performance measures (Saxena, Celaya, et al., 2008) among which accuracy-based measures such as the *timeliness*, also called scoring function in the sequel since it has been used in the data challenge to sort participants algorithm. The review of papers using the C-MAPSS datasets show that the timeliness was the most used performance measure (about 30% of papers). Note that, for datasets $\#5_T$ and $\#5_V$, this performance measure is returned for each submission by the data challenge chairs.

For comparison purpose, the scoring function is also used in this paper with the same parameters as in the challenge:

$$S = \sum_{n=1}^{N} S_n \tag{10a}$$

$$S_n = \begin{cases} e^{-d_n/13} - 1, d_n \leq 0 \\ e^{d_n/10} \quad - 1, d_n > 0 \end{cases}, n = 1 \dots N \tag{10b}$$

$$d_n = \text{estimated RUL} - \text{true RUL} \tag{10c}$$

This function, that assigns higher penalty to late predictions, has to be minimised. In addition to the scoring function (computed for all datasets), a second performance measure was used (on datasets $\#1$ to $\#4$ for which we know the RUL) called accuracy measure A that evaluates the percentage of testing instances for which the RUL estimate is within the interval $[-13, +10]$ around the true RUL (Saxena, Celaya, et al., 2008). These values are the same as the scoring function and was used in several papers such as (Ramasso et al., 2013) for dataset $\#1$.

3.3. Related results on C-MAPSS

For comparison purpose, results of predictions from other researchers (as exhaustive as possible) on these datasets are summarised below for each dataset. Note that some authors also used the simulator to create their own datasets (Sarkar, Jin, & Ray, 2011; Zein-Sabatto, Bodruzzaman, & Mikhail, 2013; Al-Salah, Zein-Sabatto, & Bodruzzaman, 2012). References have been put on the NASA PCOE website.

To our knowledge, the full testing dataset of $\#1$ was only used in two papers: In (Liu, Gebraeel, & Shi, 2013) where

Datasets	C-MAPSS DATASETS					
	TURBFOFAN				CHALLENGE	
	#1	#2	**#3**	#4	$\#5_T$	$\#5_V$
Nb. of faults	1	1	2	2	1	1
Nb. of operating conditions	1	6	1	6	6	6
Nb. training instances	100	260	100	249	218	
Nb. testing instances	100	259	100	248	218	435
Minimum RUL	7	6	6	6	10	6
Maximum RUL	145	194	145	195	150	190

Table 1. Datasets characteristics according to the organisers. In this paper, results for all datasets are provided in the experiments, but more details are given specifically for datasets $\#1$ and $\#3$. Note that the datasets called "data challenge" have a common training datasets made of 218 instances. The "semi-final" testing dataset ($\#5_T$) is made of 218 instances and the "final" validation dataset ($\#5_V$) is made of 435 instances.

the authors reported results by using an average error between true RUL and prediction; and to evaluate the EVIPRO algorithm in (Ramasso et al., 2013) where the performance was assessed by using the accuracy measure which was equal to 53% on the testing dataset $\#1$. The full testing datasets of $\#2$, $\#3$, $\#4$ were not used in the past (only a few instances were considered in a few papers).

Testing datasets $\#5_T$ (corresponding to a "semi-final" testing dataset) and $\#5_V$ (corresponding to the "final" validation dataset) represent datasets for which the true RULs is *not known*. These datasets were used in many papers summarised in Table 2 (for published work after 2008) and in Table 3 (for results of challengers during the competition in 2008). The complete review of scores on these datasets were found on the web or obtained by request to the conference chairs. In Table 3, methods (1), (2) and (3) were published in (T. Wang et al., 2008), (Heimes, 2008) and (Peel, 2008) respectively.

It can be observed that no score has been mentioned in the literature on the final validation dataset $\#5_V$ since 2008, whereas the semi-final testing dataset $\#5_T$ was used in several papers. The final dataset is complex and the performances obtained by the challengers are high. According to our knowledge, good performances (in terms of scoring) can be obtained on the final dataset only if the algorithm is robust. Indeed, a few important mistakes (too late or too early predictions) can lead to bad scores. This was also observed with RULCLIPPER on the other datasets. Robustness can be evaluated by computing several PHM metrics (Saxena, Celaya, et al., 2008) as proposed in (T. Wang, 2010).

Therefore, the generalisation capability of the algorithm should be ensured before trying the final dataset. This is illustrated in Tables 2-3 and Figure 6 which depict the scores obtained on the semi-final dataset $\#5_T$ and on the final dataset $\#5_V$. Some algorithms exhibited very low score on $\#5_T$ (made of 218 instances), whereas a relatively poor score was obtained on the final dataset. The winner obtained 737 on $\#5_T$ (according to the conference chairs) which is not the best score, but only 5636 on the final dataset $\#5_V$.

Algo. (pseudo.)	$\#5_T$	$\#5_V$
RULCLIPPER	**752**	**11572**
SBL (P. Wang, Youn, & Hu, 2012)	1139	n.a.
DW (Hu, Youn, Wang, & Yoon, 2012)	1334	n.a.
OW (Hu et al., 2012)	1349	n.a.
MLP (Riad, Elminir, & Elattar, 2010)	1540	n.a.
AW (Hu et al., 2012)	1863	n.a.
SVM-SBI (Hu et al., 2012)	2047	n.a.
RVM-SBI (Hu et al., 2012)	2230	n.a.
EXP-SBI (Hu et al., 2012)	2282	n.a.
GPM3 (Coble, 2010)	2500	n.a.
RNN (Hu et al., 2012)	4390	n.a.
REG2 (Riad et al., 2010)	6877	n.a.
GPM2B (Coble, 2010)	19200	n.a.
GPM2 (Coble, 2010)	20600	n.a.
GPM1 (Coble, 2010)	22500	n.a.
QUAD (Hu et al., 2012)	53846	n.a.

Table 2. Performance of the state-of-the-art approaches on $\#5_T$ (semi-final dataset) and $\#5_V$ (final dataset) after 2008 (published work).

Note that some papers using the datasets of the data challenge are not mentioned in the table because error measures (accuracy-based) were given and that is not possible by using the original testing datasets for which the *true RULs are not known*: testing errors are not possible on testing datasets $\#5_T$ and 5_V, but only on the training dataset. This rule (defined from 2008 to 2014) may change in the near future so that other metrics (in addition to the scoring function) could be obtained on demand to the data challenge chairs.

3.4. Priors about the datasets

Some rules were used to improve prognostics on these datasets, some have been proposed in previous papers:

R1: The first rule is related to the fact that, according to (Saxena, Goebel, et al., 2008), the maximum RUL in testing instances for $\#5_T$ was greater than 10 and lower than 150 time-units, while being greater than 6 and greater than 190 in testing instances for $\#5_V$. Moreover, most of previous approaches agreed on limiting the RUL estimates around 135 (depending on papers (T. Wang et al., 2008;

Algo. (pseudo.) / Data	$\#5_T$	$\#5_V$
heracles (1)	737 (3rd)	5636 (1st)
FOH (2)	512 (2nd)	6691 (2nd)
LP (3)	n.a.	25921
sunbea	436.8 (1st)	54437 (22nd)
bobosir	1263	8637
L6	1051	9530
GoNavy	1075	10571
beck1903	1049	14275
Sentient	809	19148
A	975	20471
mjhutk	2430	30861
RelRes	1966	35863
phmnrc	2399	35953
SuperSiegel	1139	154999

Table 3. Pseudonyms and scores (known on *both* $\#5_T$ and $\#5_V$) during the 2008's PHM data challenge. Methods (1), (2) and (3) were published

T. Wang, 2010; Heimes, 2008; Riad et al., 2010)) because too large and late estimates are greatly penalized by the scoring function. So, for most of tests presented below, the RUL was given by $\max(6, \min(\hat{\text{RUL}}, 135))$ where $\hat{\text{RUL}}$ was the estimated RUL.

R2: The difference between 1 and the average of the first 5% of an instance was used as an offset to compel the health index (HI) to begin around 1. Even though the health index function (Eq. 11) already compels it, there are some cases, in particular for #2, #3 and #4, for which the health index was strongly disturbed by fault modes and operating conditions.

R3: To limit the impact of fault modes (datasets #3 and #4), a detection of the monotonicity (Coble, 2010) is performed. When the testing instance is less than the half of the training instance and if more than 25 consecutive samples are above the training instance, then the training instance is not taken into account. This simple rule was applied on all datasets considered (even without fault modes or without operating conditions).

R4: To decrease the risk of overpredictions, the sequence of states $\mathcal{K}$ were made of two states, the second state being activated only 15 samples before the end-of-life. This setting similar to (Ramasso & Gouriveau, 2013), was the same for all tests and all datasets.

3.5. Local/global health index estimation

To reflect a real-world and practical cases, the health indices (HI) for both training and testing datasets were not given by the organisers (Saxena, Goebel, et al., 2008). An adaptation of the approach proposed in (T. Wang, 2010) is presented below to estimate the HI for each instance. These HIs (highly corrupted by noise) are the basis of the proposed methodology described in previous sections (Fig. 4).

The set of features for the ith unit is $\mathbf{X}_i = [\mathbf{x}_1\ \mathbf{x}_2 \ldots \mathbf{x}_t \ldots \mathbf{x}_{T_i}]^{\mathrm{T}}$ where $\mathbf{x}_t = [x_{t,1}\ x_{t,2} \ldots x_{t,m} \ldots x_{t,q}]$ is the q-dimensional feature vector at t (composed of sensor measurements), and $\mathbf{u}_t$ is the vector of operating conditions at t. The operational conditions variables can be clustered into a finite number of operating regimes (T. Wang, 2010). Crisp outputs are obtained such that the current regime at time t, C_t, is precisely known. Then, for samples $(\mathbf{u}_t, \mathbf{x}_t)$ collected at early age of the system, e.g. $t < \sigma_1$, the health index attached to the ith training unit is $\text{HI}(\mathbf{x}_t, \boldsymbol{\theta}^p) = 1$, where the set of parameters $\boldsymbol{\theta}^p$ depends on the model used to link regimes and sensor measurements.

At late age of the system, e.g. $t > \sigma_2$, the corresponding output is $\text{HI}(\mathbf{x}_t, \boldsymbol{\theta}^p) = 0$. In (T. Wang, 2010), the author used only the data at $t > \sigma_2$ and $t < \sigma_1$ in addition to 6 models (one for each operating mode) built on all data. In comparison, we propose to make use of samples between σ_1 and σ_2 while building a local model for each operating mode in each training instance. Moreover, we have used one HI for each training instance while in (T. Wang, 2010) a global HI model was estimated using all instances.

The corresponding output of the index is set to

$$\hat{\text{HI}}_i(\mathbf{x}_t, \boldsymbol{\theta}^p) \equiv 1 - \exp\left(\frac{\log(0.05)}{0.95 \cdot T_i} \cdot t\right) \ , t \in [\sigma_1, \sigma_2]. \quad (11)$$

This function allows to compel the health index to be globally decreasing, from 1 (healthy) to 0 (faulty). As proposed in (T. Wang, 2010), $\sigma_1 = T_i \cdot 5\%$ and $\sigma_2 = T_i \cdot 95\%$ where T_i is the length of the ith training instance. We used local linear models for multi-regime health assessment so that $\boldsymbol{\theta}_i^p = [\theta_{i,0}^p\ \theta_{i,1}^p \ldots \theta_{i,q}^p]$ represents the parameters of a linear model defined conditionnally to the pth regime. The health index at time t given the pth regime can be estimated as

$$\text{HI}_i(\mathbf{x}_t, \boldsymbol{\theta}_i^p) = \theta_{i,0}^p + \sum_{n=1}^{q} \theta_{i,n}^p \cdot x_{t,n} \quad (12)$$

where $\boldsymbol{\theta}^p$ can be estimated by standard least-squares algorithms. In experiments, in case the estimation of HI is performed by considering the three operating conditions, then it will be called a *local* approach (Fig. 4) and *global* otherwise. HIs are then transformed into IHIs as proposed in previous sections (Fig. 4).

3.6. Information fusion for improved RUL estimation

The first family of rules is a combination of minimum and maximum RUL estimates suggested in (T. Wang, 2010):

$$\alpha m M(R) = \alpha \cdot \min R + (1 - \alpha) \cdot \max R \quad (13)$$

where R is a set of RUL estimates and $\alpha m M(R)$ the combination result. For example, in (T. Wang, 2010), $\alpha = 13/23$. In this paper, we considered $\alpha \in \{0.1, 0.2, 0.3, \ldots 0.9, 13/23\}$. The authors in (T. Wang, 2010) also added two outlier removal (OR) rules to keep RULs within the interquartile range:

$$OR : \{a \in R : a \in [q_{25}, q_{75}]\} \tag{14}$$

and

$$WL : \{a \in R : q_{50} - 3\cdot(q_{50} - q_{25}) < a < q_{50} + 2\cdot(q_{75} - q_{50})\} \tag{15}$$

The set of RUL estimates provided by the algorithm, considering either discrete ($\mathcal{K}$) or continuous predictions ($\mathcal{P}$), is denoted

$$R \equiv \hat{\text{RUL}}_{\mathcal{P}[\mathcal{K}]}^{[OR|WL],[th],M} \tag{16}$$

Only the M first RULs estimates were taken into account (sorted according to the F_1 measure) with $M \in \{11, 15\}$ in this study. $OR|WL$ means that one of the outlier removal operators was applied. The optional parameter $[th]$ means that only training instances with F_1 measure greater than 0.5 were kept.

Weighted average is the second family of rules:

$$mw_L^{[e],[OR]} = \sum_{i=1}^{L} \omega_i^{[e],[OR]} \cdot R_{(i)} \tag{17}$$

where the weights are made dependent on the similarity $F_{1,i}$ (Eq. 8) between the testing instance and the ith training instance; $R_{(i)}$ is the ith RUL estimate in set of RULs R sorted in descending order with respect to the similarity ($F_{1,i}$) ; $L \in \{3, 5, 7, 9, 11, 15\}$ is the number of RULs kept to compute the average while applying or not the outlier removal rule OR. The weights are given by the following equations:

$$\omega_i = F_{1,i} / \sum_{k=1}^{L} F_{1,k} \ , \tag{18}$$

with softmax normalisation:

$$\omega_i^e = \exp(F_{1,i}) / \sum_{k=1}^{L} \exp(F_{1,k}) \ , \tag{19}$$

using outlier removal (OR):

$$\omega_i^{OR} = OR(F_{1,i}) / \sum_{k=1}^{L} OR(F_{1,k}) \ , \tag{20}$$

and combining OR and softmax:

$$\omega_i^{e,OR} = \exp(OR(F_{1,i})) / \sum_{k=1}^{L} \exp(OR(F_{1,k})) \ . \tag{21}$$

The third kind of rules is a combination of the previous ones:

$$\hat{\text{RUL}} = 0.5 \cdot \alpha m M(R) + 0.5 \cdot mw_L^{[e],[OR|WL]} \tag{22}$$

Considering several combinations of parameters, about 3168 rules were considered.

3.7. Selecting the subset of sensors

As shown by the literature review presented beforehand, many combinations of features can be used (among 21 variables), and a subset was particularly used made of features $\{7, 8, 12, 16, 17, 20\}$ (involving key sensors for the turbofan degradation (Sarkar et al., 2011)). To this preselection, a subset of sensors was added from every possible subsets with cardinality equal to $1, 2, 3$ and 4 in $\{\emptyset, 9, 10, 11, 13, 14, 18, 19, 22, 25, 26\}$ as well as subsets of cardinality 5 comprising sensor 9 leading to a total of 511 cases. For each combination (511 cases for each dataset), we applied the prognostics algorithm RULCLIPPER introduced previously and the best subset was selected by minimising the scoring function.

3.8. Testing datasets

Given the training instances of a given dataset, the first task is to create a testing dataset in order to estimate 1) the input features and 2) the fusion RUL of RULCLIPPER. The training instances were truncated at a time instant randomly selected from a uniform distribution between 10% and 80% of the half-remaining life. This procedure allowed to obtain instances with small enough RULs to allow the occurrence of substantial degradation, and also large enough RULs to test the robustness of algorithms (Hu et al., 2012). The obtained testing datasets were used in RULCLIPPER with all subsets of features (511 subsets, 3168 fusion rules) and with two subsets of features (511×511 combinations for each fusion rule).

4. RESULTS AND DISCUSSIONS

Results are presented and compared to past work for all datasets (turbofan and data challenge). More details are given for datasets $\#1$, $\#3$ and $\#5_T$ and $\#5_V$.

4.1. Performances on datasets $\#1$ and $\#3$

The results can be represented in the penalty – accuracy plane for all combinations of features. A point in that plane with coordinates $(P_1(S_1, A_1))$ is obtained by considering the accuracy (A_1) for the lowest penalty score (S_1) given a subset of features. In order to represent the imprecision concerning the performances, a second point $P_2(S_2, A_2)$ is taken and defined by the lowest score plus 25% ($S_2 = S_1 + 25\% S_1$) with accuracy (A_2): these two points define a rectangle in the penalty – accuracy plane.

Figure 5 represents the accumulation of these rectangles for all combinations of features in the testing datasets $\#1$ and $\#3$. The whitest part corresponds to the area where most of rectangles are located and thus to the likeliest performances given several subsets of features. If the white area is large then it means that the subset of features should be carefully selected. If the area is concentrated then several subsets of features provided similar performances: it is an image of the robustness with respect to the choice of the subsets. The scores have been divided by the number of testing instance for comparison purpose.

For dataset #1, the performance's centroid is located around $(60\%; 4.0)$ (or $(60\%; 400)$). One can draw any subset of features (among the 511 combinations considered) and can expect a score between $S = 310$ and $S = 440$ with an accuracy between $A = 56$ and $A = 64$. A few "optimal" subsets led to better performances (reported in Table 4 for the testing datasets). The effect of the fault mode on the performances is important. The scores are more spread and a clear global decrease of the accuracy is observed (translation of the cluster of performances to the left hand-side). The level of the colorbar indicates that the choice of the features becomes more and more crucial as the difficulty of the dataset increases: it is simpler to find a subset of features for dataset #1 leading to low penalty and high accuracy because the level is quite similar on a large area (with a value around 8). However, it is more sensitive for dataset #3 for which the level is around 12 on a very local area. A similar (and magnified) observation was obtained on the other datasets.

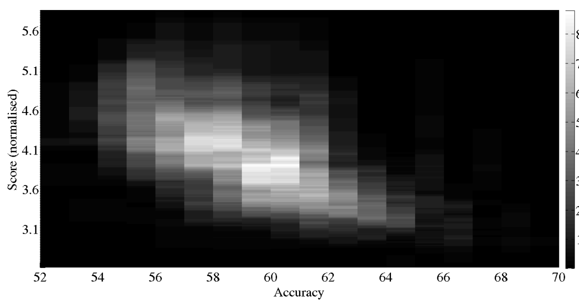

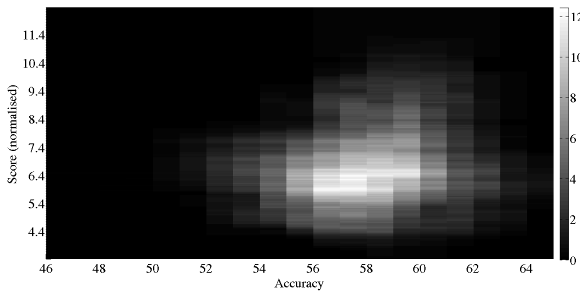

Figure 5. Performances for #1 (top) and #3 (bottom).

Based on these results obtained on the testing datasets, the fusion rule and the subset of features were selected for final evaluation of the testing datasets by minimising the scoring function (as done for the PHM data challenge) and maximising the accuracy. The results obtained on the testing datasets #1 and #3 are summarised in Table 4 (note that the features indicated in the table have to be assembled with features 7, 8, 12, 16, 17, and 20). For each dataset, the combinations of features are given with respect to the two best scores ("Best S") and the two best accuracies ("Best A"). For example, the first line of Table 4 concerns dataset #1 for which the best score is $S = 261$ (with $A = 63\%$) when using features 9, 10, 14, 25 and 26, and the RUL fusion "$0.9mM(\hat{\text{RUL}}_{\mathcal{P}}^{th,11}) \oplus mw_7$" which corresponds to the combination of two elements: 1) the output of the min/max operator (Eq. 13) with parameter $\alpha = 0.9$ applied on the 11 first RUL estimates and keeping only estimates with a similarity greater than 0.5, and 2) the weighted average (Eq. 17) of the $L = 7$ first RUL estimates after outlier removal. The high value of α (0.9) implies more weight to the minimum (early) estimate. An accuracy of 70% on #1 was obtained with the same subset of features while keeping a low score at $S = 301$. This accuracy obtained by the RULCLIPPER algorithm is significantly higher (+16%) than the previous known results given by the EVIPRO-KNN algorithm (Ramasso et al., 2013) which yielded 53%. Other metrics were computed (see Table 6) for performance comparison with previous approaches: An exponential-based regression model with health index estimation proposed in (Liu et al., 2013) that provided MAPE = 9% on #1 and an Echo State Network with Kalman filter and submodels of instances presented in (Peng et al., 2012) with[1] MSE = 3969.

The part entitled $(\#1, \#3)/S$ indicates the best scores for the same subset of features tested with the same fusion method on both datasets. Considering simultaneously #1 and #3 is equivalent to a situation where the engine is degrading while developing a fault. As the score is low and the accuracy high on both datasets using the same subset of features and the same method, it means that this parameterisation makes the prognostics robust to the introduction of the fault mode.

4.2. RULCLIPPERs ensemble to manage sensors faults

Two RULCLIPPERs were considered, each with one particular subset of features. All couples of subsets of features were studied (about 130000 combinations) on each testing dataset. The best couples are given in Table 5.

Beyond the important improvement of scores and accuracies compared to the previous results (Table 4), it shows it is not enough to take the two subsets leading to the two best results and expecting an improvement of the performances. Indeed, in most cases, performances for the single feature subsets selected are not the best ones, but their combination yielded to significative improvement of the performances compared to Table 4. For example, for dataset #1, combining RUL estimates provided by subset of features $\{10, 11, 14, 22\}$ (in addition to 7, 8, 12, 16, 17, 20) with $\{13, 18, 19, 22\}$ led to $S = 216$ and $P = 67\%$. It represents 27% of improvement on the score and +4% on accuracy compared to the best per-

[1]Authors in (Peng et al., 2012) actually provided the best RMSE obtained equal to 63, so MSE was computed as $3969 = 63^2$.

TYPE	DATA	FEATURES	FUSION	S	A
Best /S	$\#1$	$9, 10, 14, 25, 26$	$0.9mM(\hat{\text{RUL}}_{\mathcal{P}}^{th,11}) \oplus mw_7$	272	68
Best /A	$\#1$	$9, 10, 14, 25, 26$	$0.9mM(\hat{\text{RUL}}_{\mathcal{P}}^{th,11}) \oplus mw_{13}$	301	70
Best /S	$\#3$	$9, 13, 14, 22, 26$	$0.9mM(\hat{\text{RUL}}_{\mathcal{PK}}^{WL,11}) \oplus mw_3^{OR}$	353	57
Best /A	$\#3$	$9, 19, 25$	$0.8mM(\hat{\text{RUL}}_{\mathcal{PK}}^{WL,11})$	632	63
Best /A (2)	$\#3$	$18, 25, 26$	$mw_{e,5}^{e,OR} \oplus mw_5$	580	63
Best /A (3)	$\#3$	$9, 10, 14, 18, 25$	$0.8mM(\hat{\text{RUL}}_{\mathcal{PK}}^{WL,11}) \oplus mw_3$	476	60
$(\#1, \#3)$ /S	$\#1$	$9, 11, 14, 25, 26$	$0.9mM(\hat{\text{RUL}}_{\mathcal{P}}^{th,11}) \oplus mw_9^{e,OR}$	294	64
	$\#3$	$-$	$-$	480	55
$(\#1, \#3)$ /S(2)	$\#1$	$9, 10, 14, 25, 26$	$0.9mM(\hat{\text{RUL}}_{\mathcal{P}}^{th,11}) \oplus mw_{13}^{OR}$	299	63
	$\#3$	$-$	$-$	480	56
$(\#1, \#3)$ /S(2)	$\#1$	$9, 10, 14, 25, 26$	$0.9mM(\hat{\text{RUL}}_{\mathcal{P}}^{th,11}) \oplus mw_5^{OR}$	315	66
	$\#3$	$-$	$-$	435	54

Table 4. Subset of features (in addition to 7, 8, 12, 16, 17, 20) leading to the best performances in terms of scores (and the corresponding accuracies) for each dataset using a single RULCLIPPER.

Data	Type	Features						Fusion	S	P
		Subset 1	S_1	P_1	Subset 2	S_2	P_2			
$\#1$	Best /S	$10, 11, 14, 22$	301	64	$13, 18, 19, 22$	325	62	$0.9mM(\hat{\text{RUL}}_{\mathcal{P}}^{th,11}) \oplus mw_5^{OR}$	**216**	67
	Best /A	$10, 11, 14, 22$	301	64	$13, 18, 19, 22$	325	62	$0.9mM(\hat{\text{RUL}}_{\mathcal{P}}^{th,11}) \oplus mw_7^{OR}$	224	**70**
$\#3$	Best /S	$13, 19, 25, 26$	525	61	$9, 13, 14, 22, 26$	353	58	$0.9mM(\hat{\text{RUL}}_{\mathcal{P}}^{th,11})$	**317**	59
	Best /A	$14, 18, 19, 26$	499	61	$9, 10, 13, 14, 26$	399	58	$0.9mM(\hat{\text{RUL}}_{\mathcal{P}}^{WL,15}) \oplus mw_{11}^{OR}$	332	**63**

Table 5. Combination of subsets of features (in addition to 7, 8, 12, 16, 17, 20) leading to the best performances in terms of scores (and the corresponding accuracies) for each dataset using the fusion of two RULCLIPPERs.

formances obtained in Table 4 with subset $\{13, 14, 18, 25\}$, and more when considering the performances of single subsets ($S_1 = 301$ and $P_1 = 64\%$, or $S_2 = 325$ with $P_2 = 62\%$). Similar observations can be made on $\#3$.

4.3. Results on the PHM data challenge ($\#5_T, \#5_V$)

Based on the 218 training instances provided, RULCLIPPER was run on the testing dataset using the 511 combinations of features with the 3168 fusion rules. The results were sorted by ascending order with respect to the scoring function. The first five best subsets of features were then selected: $\{9, 11, 26\}$, $\{9, 18, 22, 25\}$, $\{9\}$, $\{9, 10, 13, 25\}$, $\{9, 10, 18, 25, 26\}$ (in addition to $7, 8, 12, 16, 17, 20$ for each subset).

These combinations of features were considered and evaluated on the dataset $\#5_T$. The best score was given by averaging three configurations of RULCLIPPERs, each with ensembles based on three subsets of features:

- RULCLIPPER 1 with inputs $\{9, 11, 26\}$, $\{9, 18, 22, 25\}$ and $\{9\}$;
- RULCLIPPER 2 with inputs $\{9, 11, 26\}$, $\{9, 18, 22, 25\}$ and $\{9, 10, 13, 25\}$;
- RULCLIPPER 3 with inputs $\{9, 11, 26\}$, $\{9, 18, 22, 25\}$ and $\{9, 10, 18, 25, 26\}$.

The RUL limit was set to 135 as described in Section 3.4 and the fusion rule was the same for all individual RULCLIPPER, namely $0.9mM(\hat{\text{RUL}}_{\mathcal{PK}}^{11}) \oplus mw_{15}^{OR}$. The score obtained on dataset $\#5_T$ (on the NASA's website) was equal to 752, which is the 3rd score compared to published works. An alternative was considered by increasing the RUL limit from 135 to 175. The fusion rule was the same as previously and the score obtained was 934 which is quite low relatively to the high risk taken by setting the RUL limit to 175.

The average of the three configurations given above provided a set of RULs parameterised by both a RUL limit $(135, 175)$ and a fusion method. Three parameterisations were considered and combined: $\Omega_1 = (135, 0.8mM(\hat{\text{RUL}}_{\mathcal{PK}}^{11}) \oplus mw_5^{OR})$, $\Omega_2 = (175, 0.9mM(\hat{\text{RUL}}_{\mathcal{PK}}^{11}) \oplus mw_9^{OR})$, and $\Omega_3 = (175, 0.9mM(\hat{\text{RUL}}_{\mathcal{PK}}^{11}) \oplus mw_{15})$. The motivation of this configuration was to make long-term predictions possible while minimising the risk of making late predictions. The RULs obtained by Ω_2 and Ω_3 were averaged and the resulting combined by a weighted average with with Ω_1. The weights were set by a sigmoid (with shape parameter: 0.3 and position: 120) to increase the importance of RULCLIPPERs Ω_2 and Ω_3 when the estimation is greater than 120 while giving more importance to Ω_1 otherwise.

This methodology was then applied with the final testing dataset ($\#5_V$) yielding 11672. The comparison with approaches can be quantified on Figure 6. The generalisation of RULCLIPPER parameterised as proposed in this paper is lower than the first five algorithms (see square markers on the left-hand side). Indeed, some of these algorithms provided higher scores on $\#5_T$ but lower on the final dataset $\#5_V$. One explanation accounting for the lack of generalisation capability compared to the first five algorithms may hold in the "rules" integrated in RULCLIPPER (section 3.4). These rules have been tuned according to observations on the five other datasets but may be not relevant for dataset $\#5_V$ if the statistics governing the generation of instances have been modified (Saxena, Goebel, et al., 2008). In order to show the applicability of RULCLIPPER algorithm with as less parameterisation as possible, the author intentionally kept the same settings for all datasets without distinction in particular concerning the number of fault modes or thresholds on RUL limits.

However, the generalisation is better than the 23 remaining algorithms, for which lower scores on $\#5_T$ have been obtained with higher ones on $\#5_V$ (see square markers on the right-hand side). RULCLIPPER provided a relatively low score on both datasets using the same parameters (816 on $\#5_T$ and 11672 on $\#5_V$). The authors remarked on the previous datasets ($\#1$ to $\#4$) that a few instances can disturb the algorithm (in particular to test the robustness), generating very late or very early predictions, degrading drastically the scores. The important difference on scores between $\#5_T$ and $\#5_V$ can be due to this particularity.

A summary of results of RULCLIPPER on C-MAPSS datasets is given in Table 6. The best performances were selected according to the scoring function (better accuracies can be obtained as shown in previous tables but with lower scores). Metrics are defined in (Saxena, Celaya, et al., 2008).

5. CONCLUSION

The RULCLIPPER algorithm is proposed to estimate the remaining lifetime of systems in which noisy health indices are assumed imprecise. RULCLIPPER is made of elements inspired from both the computer vision and computational geometry communities and relies on the adaptation of case-based reasoning to manage the imprecise training and testing instances. The combination of these elements makes it an original and efficient approach for RUL estimation as shown in experiments.

RULCLIPPER was validated with the six datasets coming from the turbofan engine simulator (C-MAPSS), including the so-called turbofan datasets (four datasets) and the data challenge (two datasets), and compared to past work. These datasets are considered as complex due to the presence of fault modes and operating conditions. In addition to RULCLIPPER, a method was proposed to estimate the health indicator (in presence of faults and operating conditions) and the problem of the selection of the most relevant sensors was also tackled. Information fusion rules were finally studied to combine RUL estimates as well as ensemble of RULCLIPPERs. The review of past work, the presentation of the datasets, as well as the results on sensor selection, health index estimation, information fusion rules and RULCLIPPER ensembles are expected to give a hand to other researchers interested in testing their algorithms on these datasets.

The use of the same algorithm (RULCLIPPER) for all datasets lets suppose that, more generally, computational geometry seems promising for PHM in presence of noisy HIs. However, as for all similarity-based matching algorithm (T. Wang, 2010), the computational cost associated to sort instances is the most important limitation of RULCLIPPER. Two solutions can be considered. Firstly, since operations on convex polygons are simpler (and faster), a procedure can be used to approximate the bounds and to decrease the number of segments.

The second solution concerns implementations, particularly of the intersection algorithm. Computational geometry has become a very active field in particular to improve memory and time requirements, with applications in multimedia (computer graphics such as games). CUDA implementations on processor arrays (using graphic cards) can be pointed out as a promising solution. With such implementations, real-time and anytime prognostics can be considered. The extension of RULCLIPPER to multiple health indices is also under study, in particular by using polytopes.

ACKNOWLEDGMENT

This work has been carried out in the Laboratory of Excellence ACTION through the program "Investments for the future" managed by the National Agency for Research (references ANR-11-LABX-01-01). The author also would like to thank A. Saxena and K. Goebel to produce and make available the C-MAPSS datasets.

REFERENCES

Al-Salah, T., Zein-Sabatto, S., & Bodruzzaman, M. (2012). Decision fusion software system for turbine engine fault diagnostics. In *Southeastcon, 2012 proceedings of ieee* (p. 1-6).

Beer, M., Ferson, S., & Kreinovich, V. (2013). Imprecise probabilities in engineering analyses. *Mechanical Systems and Signal Processing*.

Bentley, J., & Ottmann, T. (1979). Algorithms for reporting and counting geometric intersections. *IEEE Trans. Comput.*, *C28*, 643-647.

Chazelle, B., & Edelsbrunner, H. (1992). An optimal algorithm for intersecting line segments in the plane. *J.*

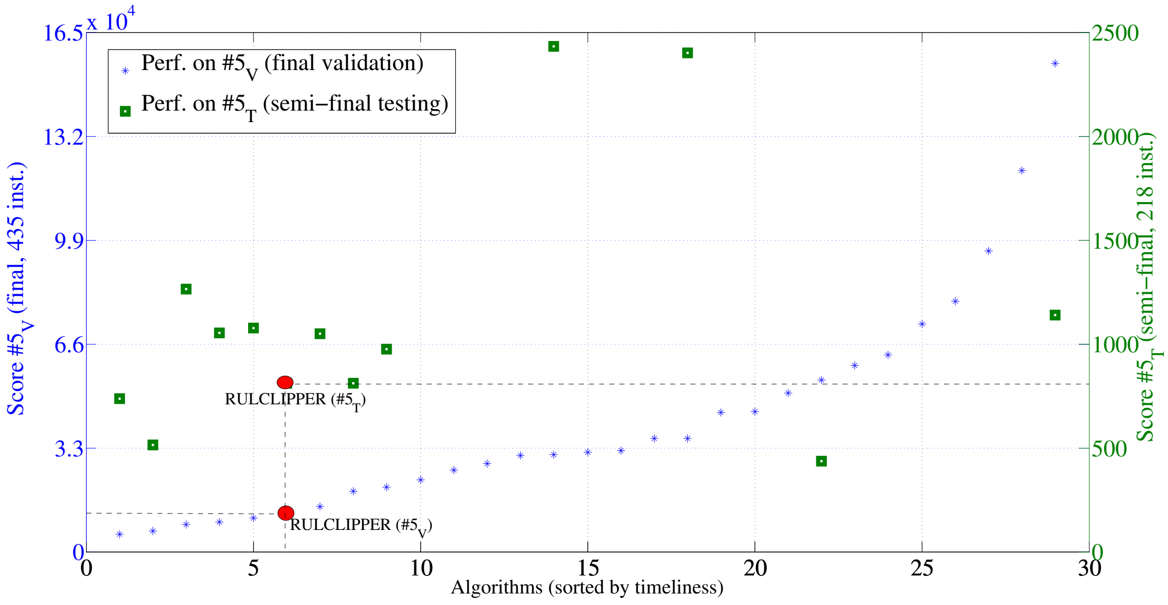

Figure 6. Comparison of RULCLIPPER with other state-of-the-art approaches. Some scores on the testing dataset $\#5_T$ are missing. Scores have to be minimised.

RULCLIPPER performance						
Dataset	$\#1$	$\#2$	$\#3$	$\#4$	$\#5_T$	$\#5_V$
Score	216	2796	317	3132	752	11672
Accuracy (%)	67	46	59	45	n.a.	n.a.
FPR (%)	56	51	66	49	n.a.	n.a.
FNR (%)	44	49	34	51	n.a.	n.a.
MAPE (%)	20	32	23	34	n.a.	n.a.
MAE	10	17	12	18	n.a.	n.a.
MSE	176	524	256	592	n.a.	n.a.

Table 6. Summary of results.

Assoc. Comput. Mach, *39*, 1-54.

Chen, C., Zhang, B., Vachtsevanos, G., & Orchard, M. (2011). Machine condition prediction based on adaptive neuro-fuzzy and high-order particle filtering. *IEEE Transactions on Industrial Electronics*, *58*(9), 4353-4364.

Coble, J. (2010). *Merging data sources to predict remaining useful life - an automated method to identify prognostic parameters* (Unpublished doctoral dissertation). University of Tennessee, Knoxville.

El-Koujok, M., Gouriveau, R., & Zerhouni, N. (2011). Reducing arbitrary choices in model building for prognostics: An approach by applying parsimony principle on an evolving neuro-fuzzy system. *Microelectronics Reliability*, *51*(2), 310 - 320.

Filippov, A. (1950). An elementary proof of Jordan's theorem. *Uspekhi Mat. Nauk*, *5*, 173-176.

Greiner, G., & Hormann, K. (1998). Efficient clipping of arbitrary polygons. *ACM Trans. on Graphics*, *17*, 71-83.

Heimes, F. (2008). Recurrent neural networks for remaining useful life estimation. In *Ieee int. conf. on prognostics and health management.*

Hu, C., Youn, B., Wang, P., & Yoon, J. (2012). Ensemble of data-driven prognostic algorithms for robust prediction of remaining useful life. *Reliability Engineering and System Safety*, *103*, 120 - 135.

Javed, K., Gouriveau, R., & Zerhouni, N. (2013). Novel failure prognostics approach with dynamic thresholds for machine degradation. In *Ieee industrial electronics conference.*

Klir, G., & Wierman, M. (1999). Uncertainty-based information. elements of generalized information theory. In (chap. Studies in fuzzyness and soft computing). Physica-Verlag.

Kuncheva, L. I. (2004). *Combining pattern classifiers: Methods and algorithms.* Wiley-Interscience.

Liu, K., Gebraeel, N. Z., & Shi, J. (2013). A data-level fusion model for developing composite health indices for degradation modeling and prognostic analysis. *IEEE Trans. on Automation Science and Engineering*.

Longley, P., de Smith, M., & Goodchild, M. (2007). *Geospatial analysis : A comprehensive guide to principles, techniques and software tools*. Matador, Leicester.

Margalit, A., & Knott, G. (1989). An algorithm for computing the union, intersection or difference of two polygons. *Computers & Graphics*, *13*, 167-183.

Orchard, M., Kacprzynski, G., Goebel, K., Saha, B., & Vachtsevanos, G. (2008). Advances in uncertainty representation and management for particle filtering applied to prognostics. In *Int. conf. on prognostics and health management.*

Peel, L. (2008). Data driven prognostics using a Kalman filter ensemble of neural network models. In *Int. conf. on prognostics and health management.*

Peng, T., He, J., Liu, Y., Saxena, A., Celaya, J., & Goebel, K. (2012). Integrated fatigue damage diagnosis and prognosis under uncertainties. In *Annual conference of prognostics and health management.*

Powers, D. (2011). Evaluation: From precision, recall and F-factor to ROC, informedness, markedness & correlation. *Journal of Machine Learning Technologies*, *2*, 37-63.

Ramasso, E., & Denoeux, T. (2013). Making use of partial knowledge about hidden states in hidden Markov models: an approach based on belief functions. *IEEE Transactions on Fuzzy Systems*, *22*(2), 395-405.

Ramasso, E., & Gouriveau, R. (2013). RUL estimation by classification of predictions: an approach based on a neuro-fuzzy system and theory of belief functions. *IEEE Transactions on Reliability*, *Accepted*.

Ramasso, E., Rombaut, M., & Zerhouni, N. (2013). Joint prediction of observations and states in time-series based on belief functions. *IEEE Transactions on Systems, Man and Cybernetics - Part B: Cybernetics*, *43*, 37-50.

Riad, A., Elminir, H., & Elattar, H. (2010). Evaluation of neural networks in the subject of prognostics as compared to linear regression model. *International Journal of Engineering & Technology*, *10*, 52-58.

Rigaux, P., Scholl, M., & Voisard, A. (2002). *Spatial databases with application to gis* (E. Science, Ed.). Kauffman Publishers.

Rosen, K. (2004). *Handbook of discrete and computational geometry, second edition* (J. E. Goodman & J. O'Rourke, Eds.). Chapman and Hall/CRC.

Sarkar, S., Jin, X., & Ray, A. (2011). Data-driven fault detection in aircraft engines with noisy sensor measurements. *Journal of Engineering for Gas Turbines and Power*, *133*, 081602.

Saxena, A., Celaya, J., Balaban, E., Goebel, K., Saha, B., Saha, S., & Schwabacher, M. (2008). Metrics for evaluating performance of prognostic techniques. In *Int. conf. on prognostics and health management* (p. 1-17).

Saxena, A., Goebel, K., Simon, D., & Eklund, N. (2008). Damage propagation modeling for aircraft engine run-to-failure simulation. In *Int. conf. on prognostics and health management* (p. 1-9). Denver, CO, USA.

Saxena, A., Wu, B., & Vachtsevanos, G. (2005). Integrated diagnosis and prognosis architecture for fleet vehicles using dynamic case-based reasoning. In *Autotestcon* (p. 96-102).

Serir, L., Ramasso, E., & Zerhouni, N. (2012). E2GKpro: An evidential evolving multi-modeling approach for system behavior prediction with applications. *Mechanical Systems and Signal Processing*. doi: 10.1016/j.ymssp.2012.06.023

Vachtsevanos, G. (2006). Intelligent fault diagnosis and prognosis for engineering systems. Wiley, Hoboken, NJ.

Vatti, B. R. (1992). A generic solution to polygon clipping. *Communications of the ACM*, *35*, 56-63.

Wang, P., Youn, B., & Hu, C. (2012). A generic probabilistic framework for structural health prognostics and uncertainty management. *Mechanical Systems and Signal Processing*, *28*, 622 - 637.

Wang, T. (2010). *Trajectory similarity based prediction for remaining useful life estimation* (Unpublished doctoral dissertation). University of Cincinnati.

Wang, T., Yu, J., Siegel, D., & Lee, J. (2008). A similarity-based prognostics approach for remaining useful life estimation of engineered systems. In *Int. conf. on prognostics and health management* (p. 1-6).

Zein-Sabatto, S., Bodruzzaman, J., & Mikhail, M. (2013). Statistical approach to online prognostics of turbine engine components. In *Southeastcon, 2013 proceedings of ieee* (p. 1-6).

BIOGRAPHY

Dr. Emmanuel Ramasso received the B.Sc. and M.Sc. degrees in Automation Science and Engineering from the University of Savoie in 2004, and earned his Ph.D. from the University of Grenoble in 2007. He pursued with a postdoc at the Commissariat à l'Energie Atomique et aux Energies Alternatives in 2008. Since 2009, he has been working as an associate professor at the National School of Engineering in Mechanics and Microtechnics (ENSMM) at Besançon (France). His research is carried out at FEMTO-ST institute and focused on pattern recognition under uncertainties with applications to Prognostics and Structural Health Management.